Supporting Information

The effect of fluorination on the low and high frequency dielectric constants of non-polymeric organic semiconductors – towards homojunction solar cells

Neil Mallo, Shaun McAnally, Ronan Chu, Mohammad Babazadeh, Hui Jin, Paul L. Burn,* Ian R. Gentle, Paul E. Shaw*

Centre for Organic Photonics & Electronics, School of Chemistry and Molecular Biosciences, The University of Queensland, Queensland 4072, Australia

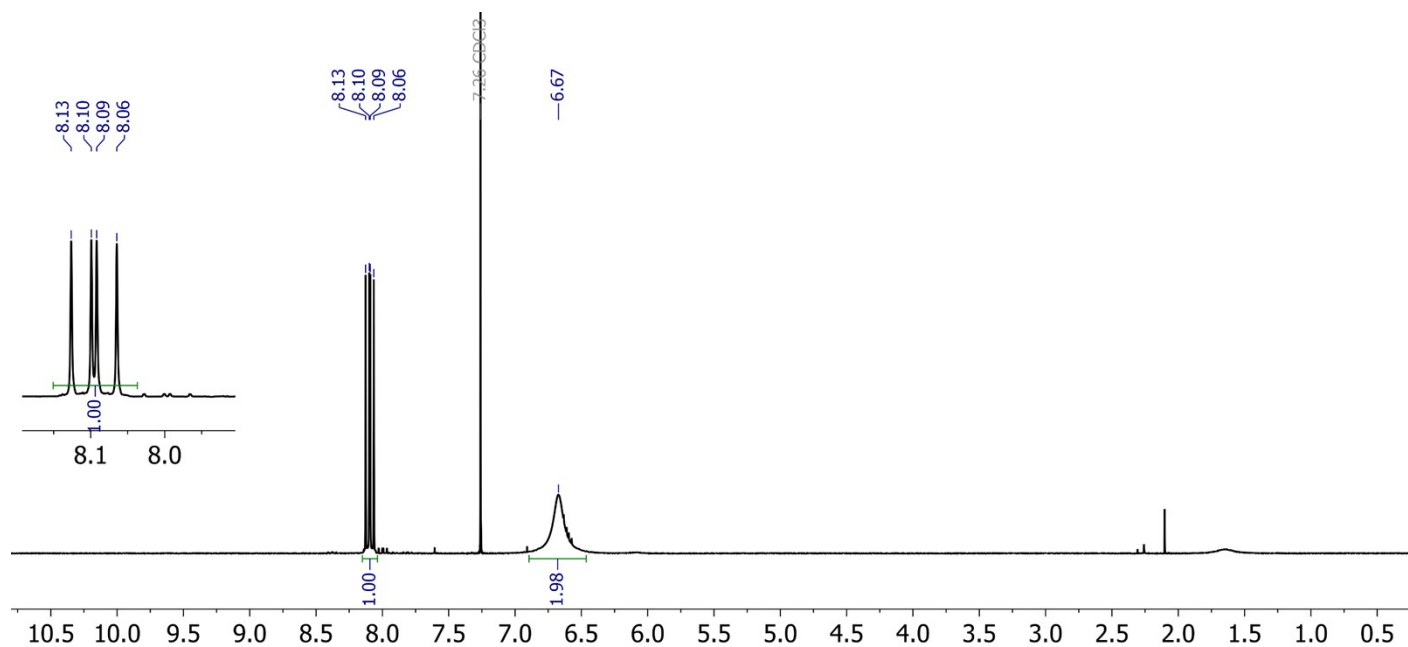*p.burn2@uq.edu.au, p.shaw3@uq.edu.au

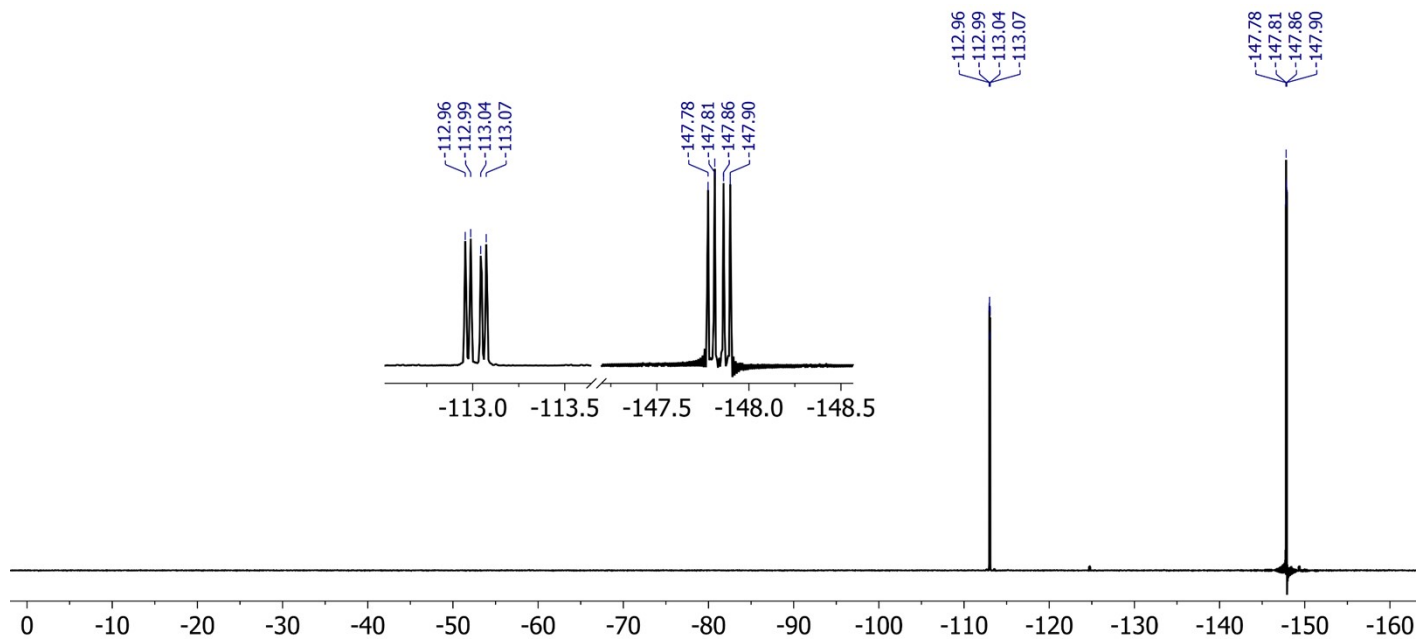**Figure S1.** ^{1}H NMR (300 MHz, CDCl$_3$) spectrum of **2**.

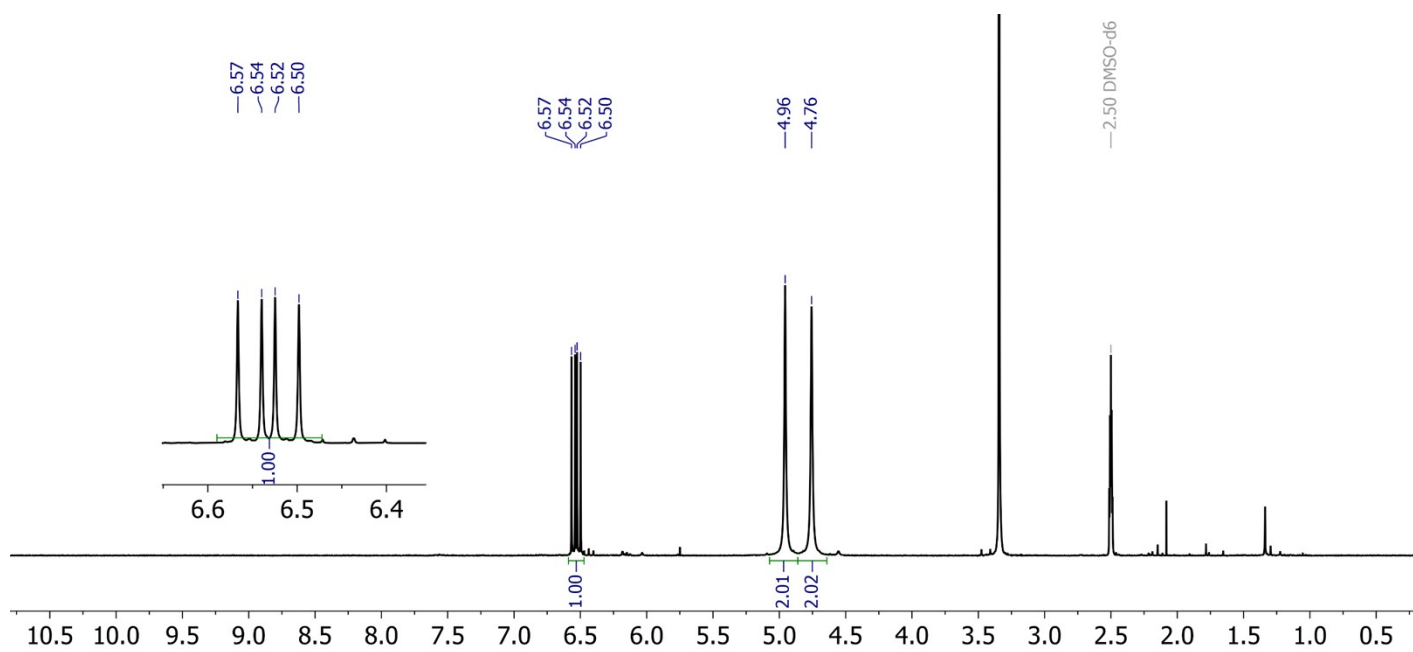**Figure S2.** ^{19}F NMR (282 MHz, CDCl$_3$) spectrum of **2**.

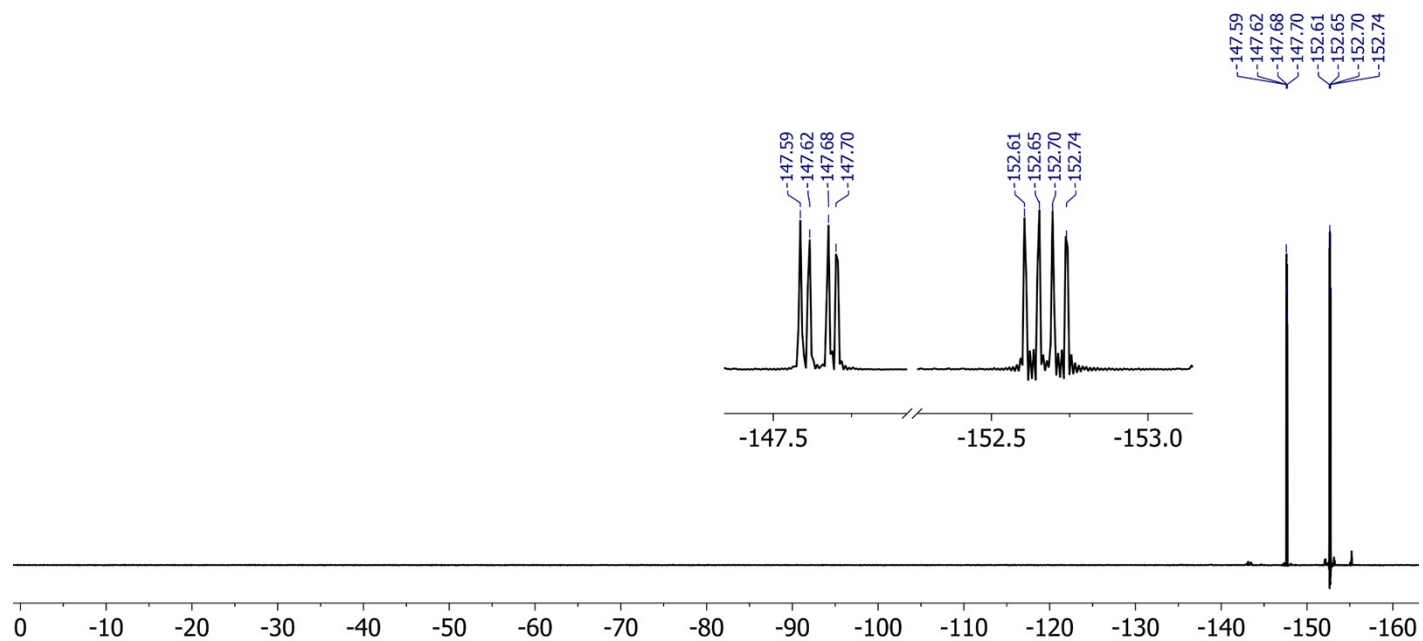**Figure S3.** ^{1}H NMR (300 MHz, DMSO-d_6) spectrum of **3**.

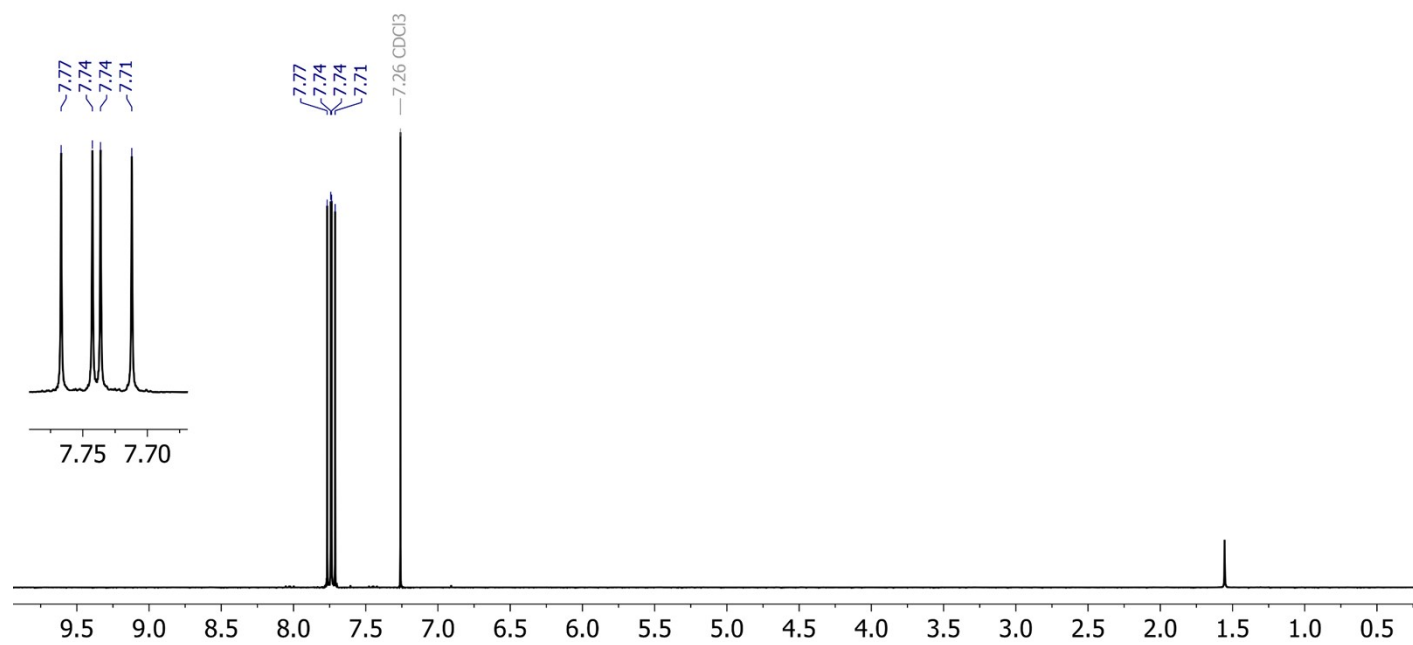**Figure S4.** ^{19}F NMR (282 MHz, DMSO-d_6) NMR spectrum of **3**.

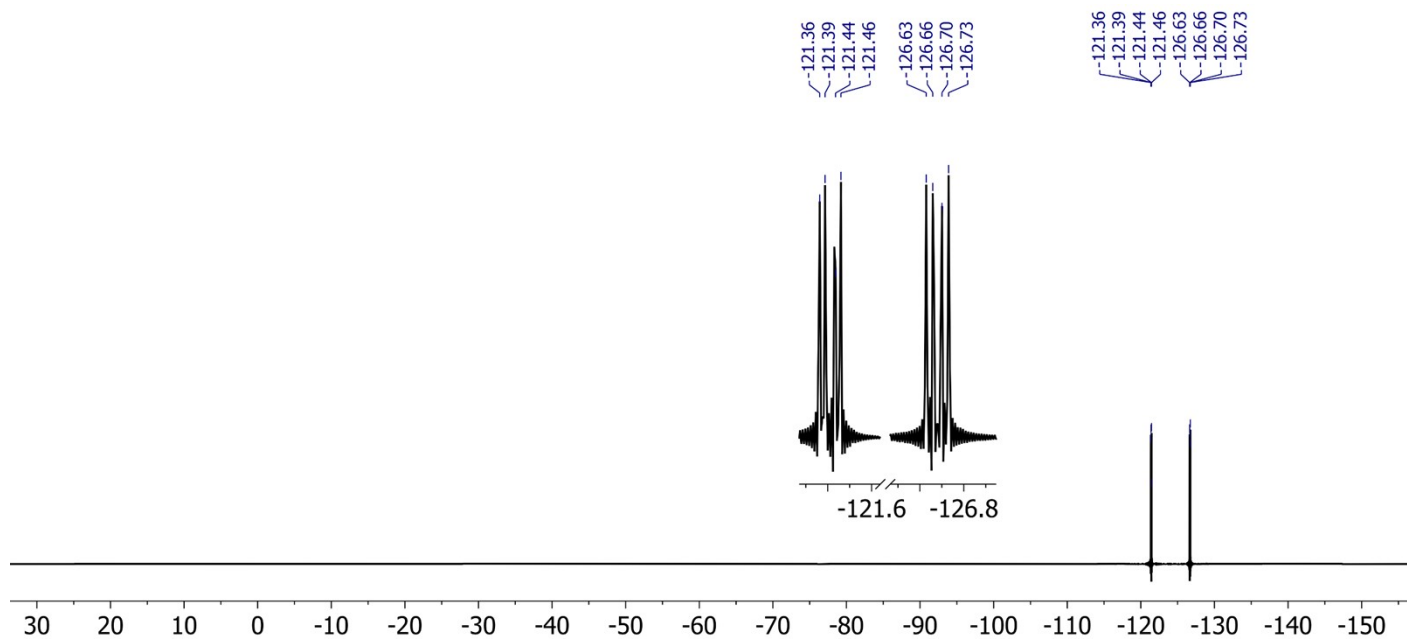**Figure S5.** ^1H NMR (300 MHz, CDCl$_3$) spectrum of **4**.

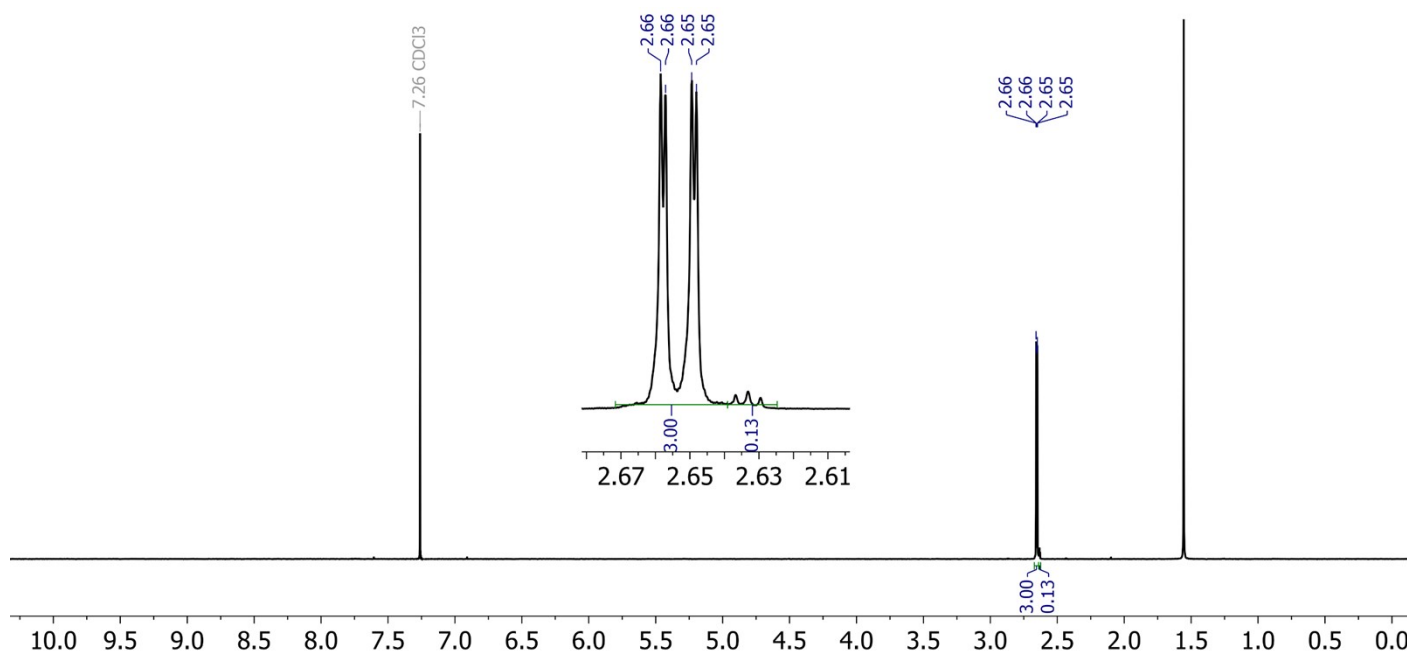**Figure S6.** ^{19}F NMR (282 MHz, CDCl$_3$) spectrum of **4**.

Figure S7. ^{1}H NMR (300 MHz, CDCl$_3$) spectrum of **5**. A trace of 5,6-difluoro-4,7-dimethylbenzo[c][1,2,5]thiadiazole remains present.
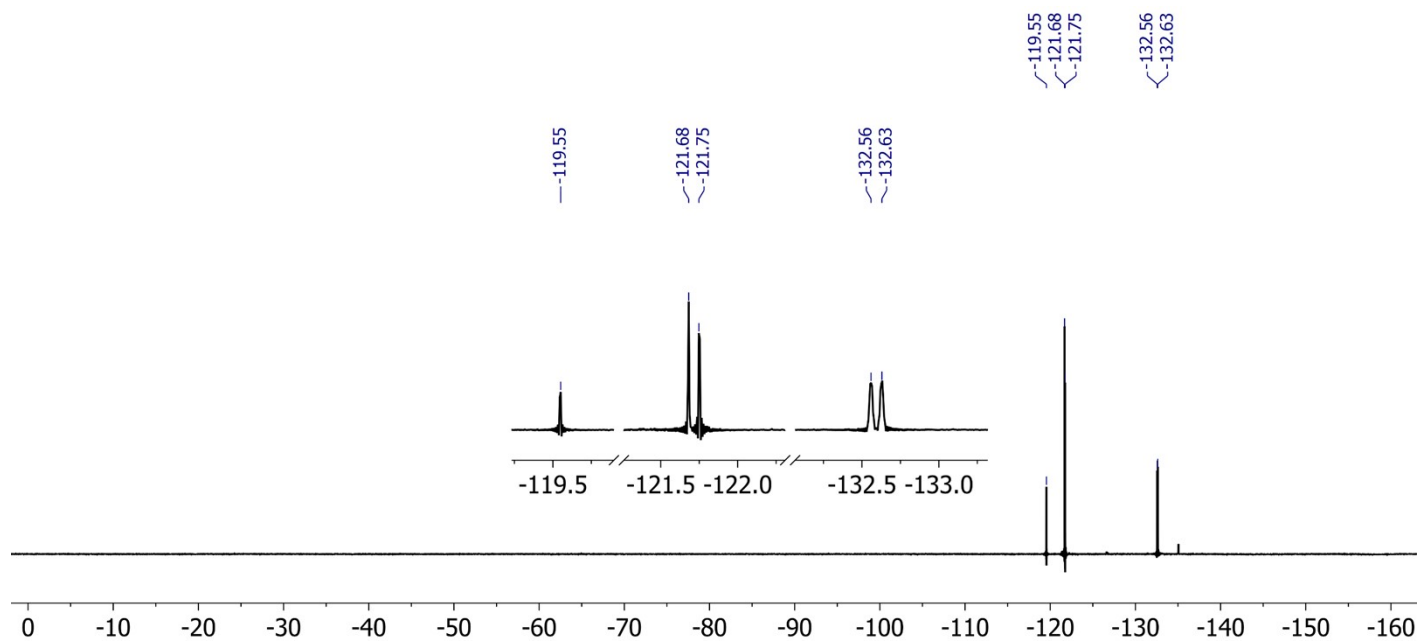
Figure S8. ^{19}F NMR (282 MHz, CDCl$_3$) spectrum of **5**. A trace of 5,6-difluoro-4,7-dimethylbenzo[*c*][1,2,5]thiadiazole remains present.
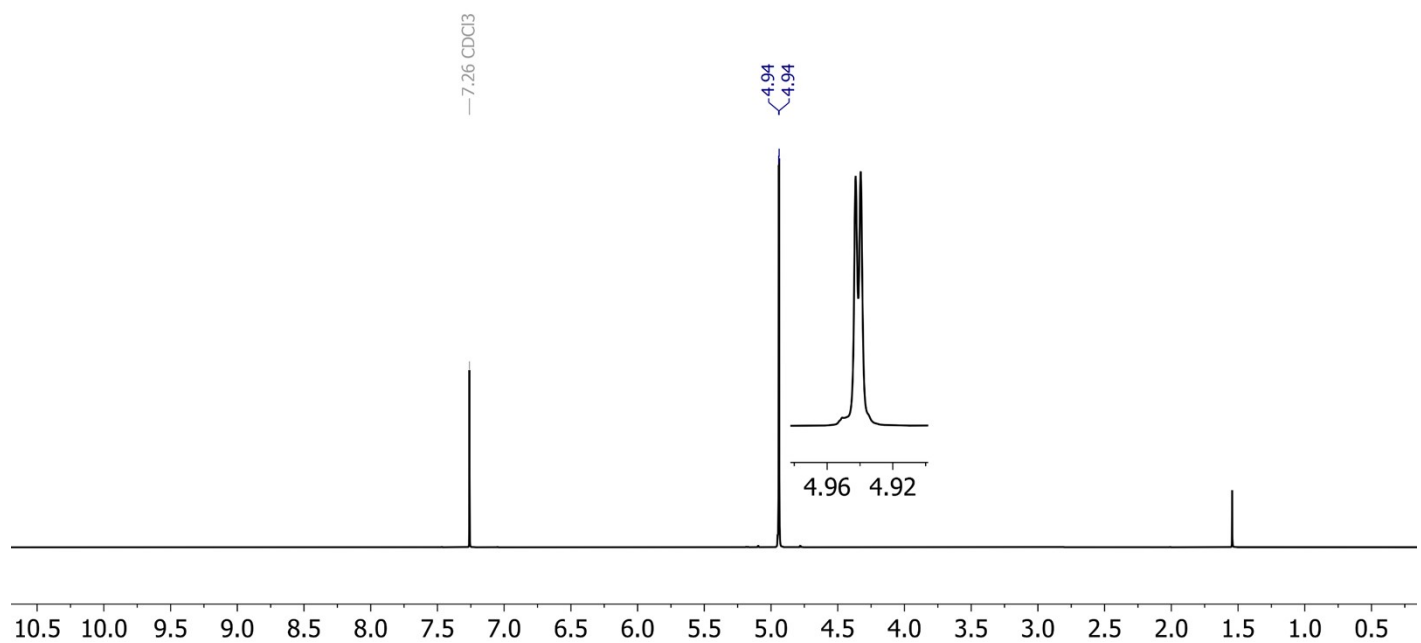

Figure S9. ^{1}H NMR (500 MHz, CDCl$_3$) spectrum of **6**. A trace of 4,7-bis(bromomethyl)-5,6-difluorobenzo[*c*][1,2,5]thiadiazole remains present.
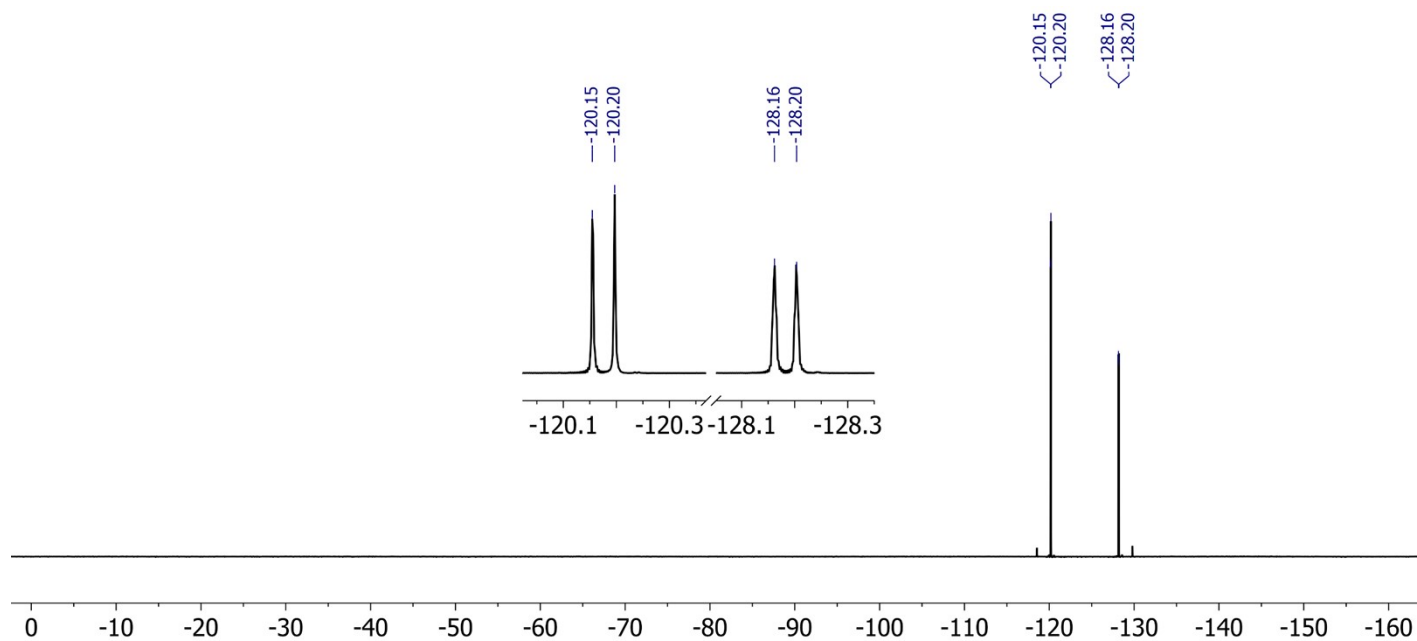
Figure S10. ^{19}F NMR (470 MHz, CDCl₃) spectrum of **6**. A trace of 4,7-bis(bromomethyl)-5,6-difluorobenzo[*c*][1,2,5]thiadiazole remains present.
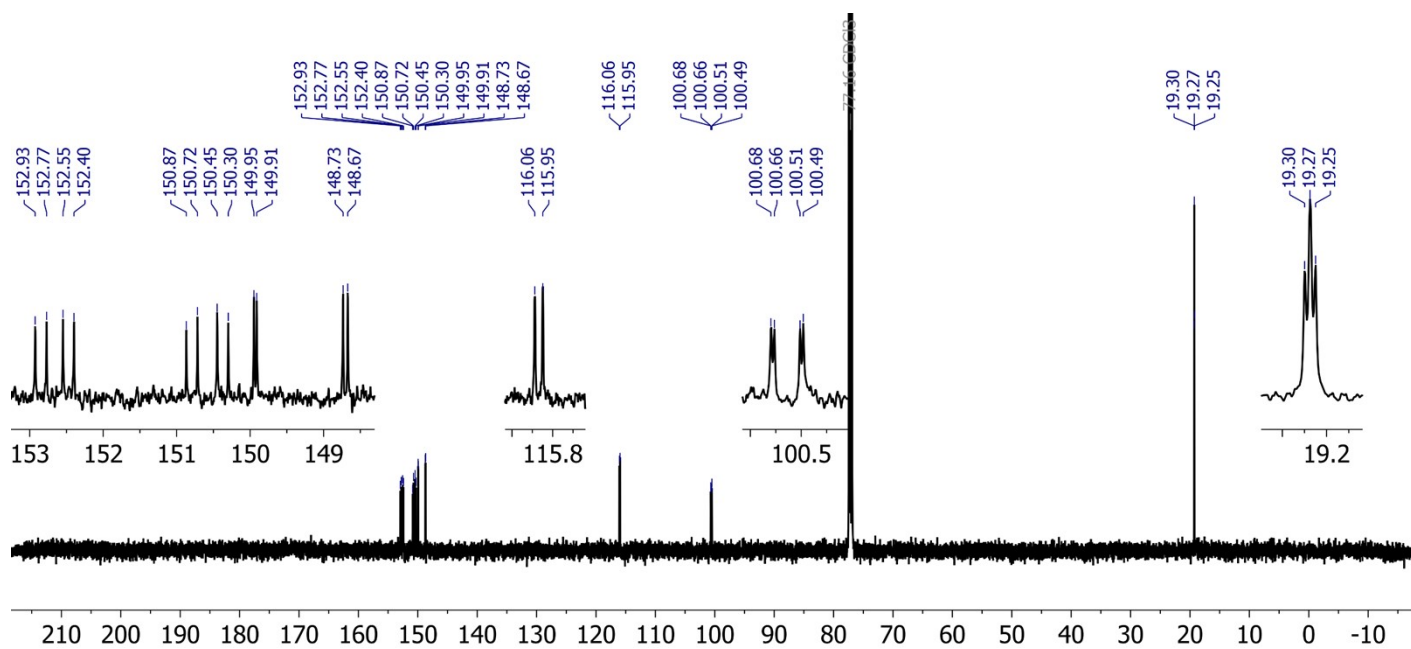
Figure S11. ^{13}C{^{1}H} NMR (126 MHz, CDCl₃) spectrum of **6**.
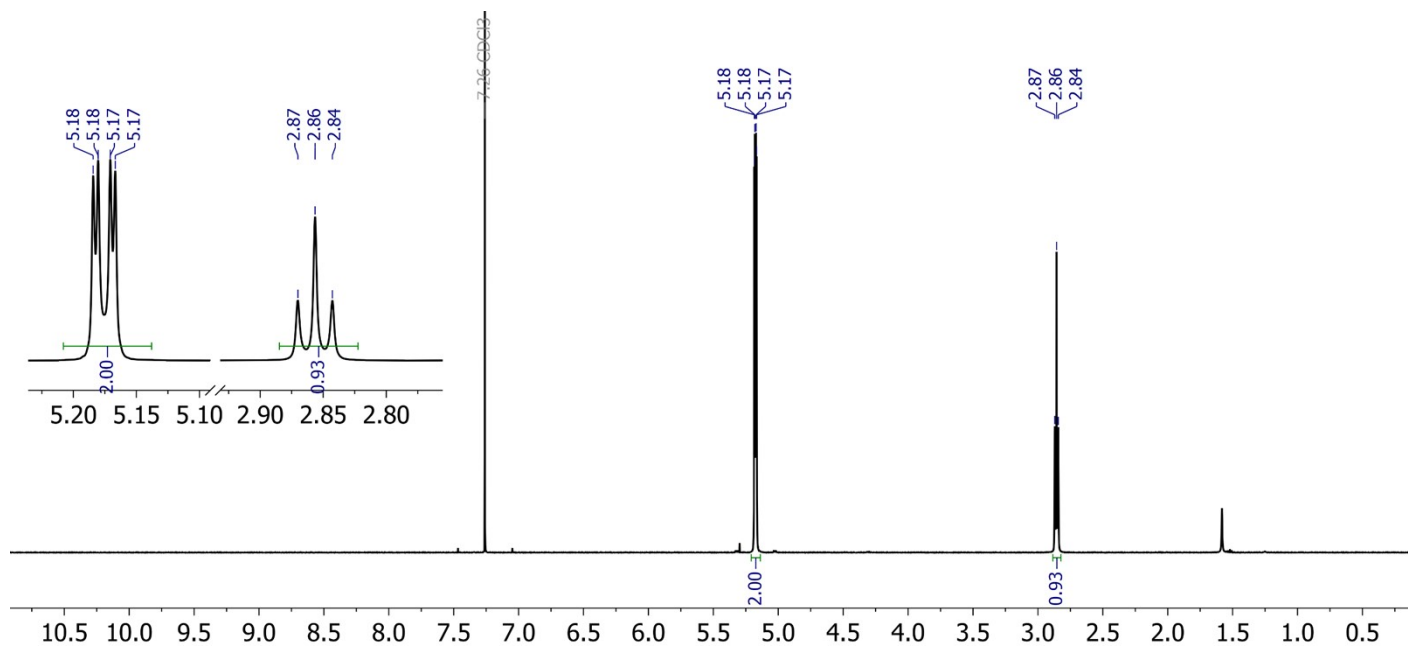
Figure S12. ^{1}H NMR (500 MHz, CDCl$_3$) spectrum of **7**.
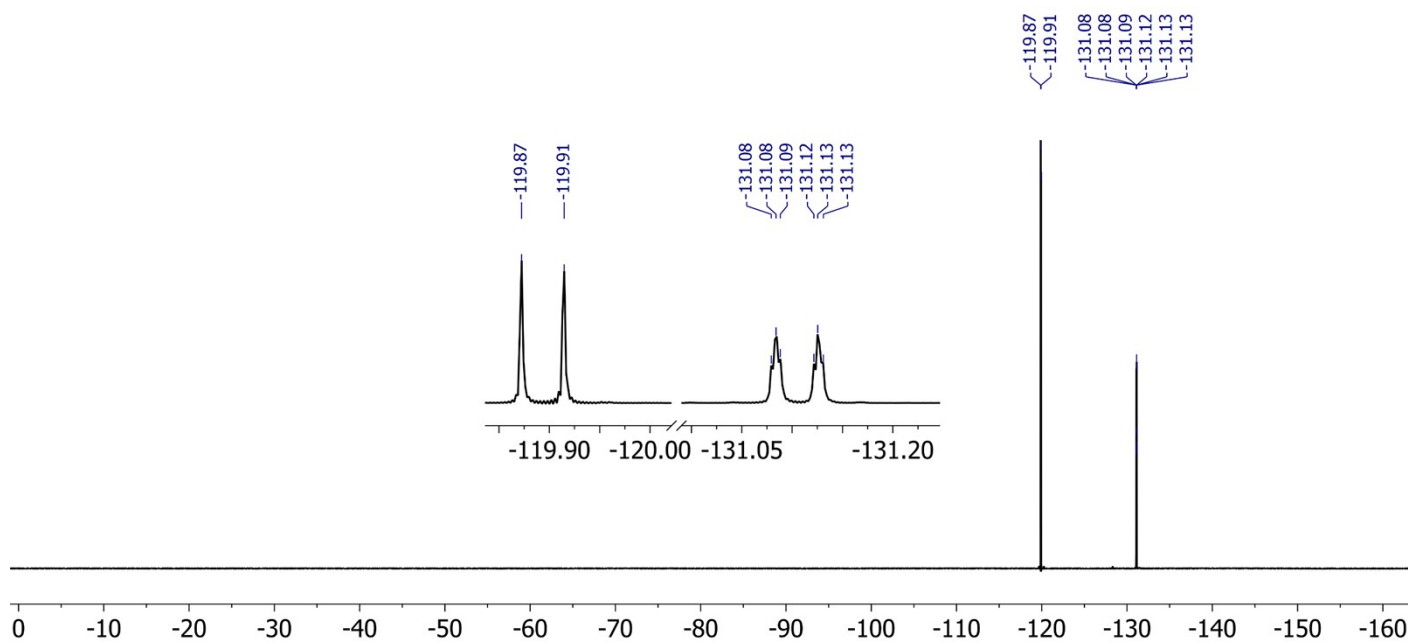
Figure S13. ^{19}F NMR (470 MHz, CDCl$_3$) spectrum of **7**.
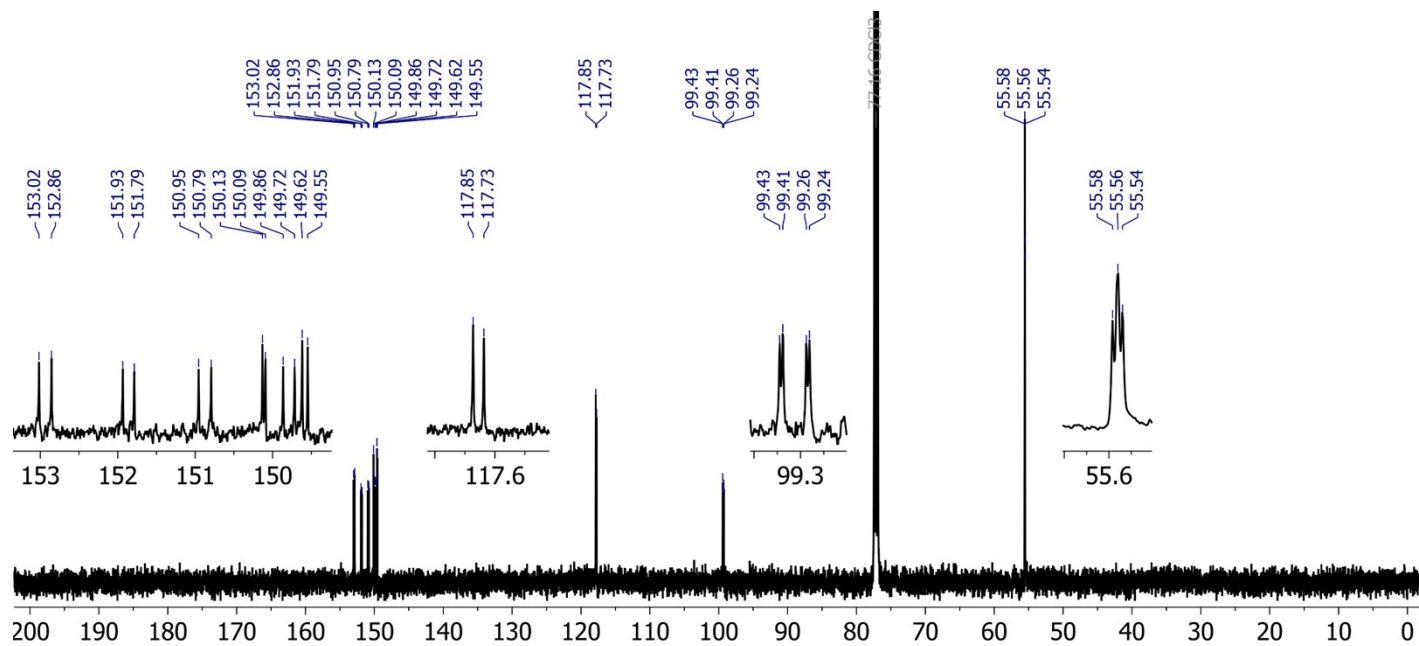
Figure S14. $^{13}C\{^1H\}$ NMR (126 MHz, CDCl$_3$) spectrum of **7**.
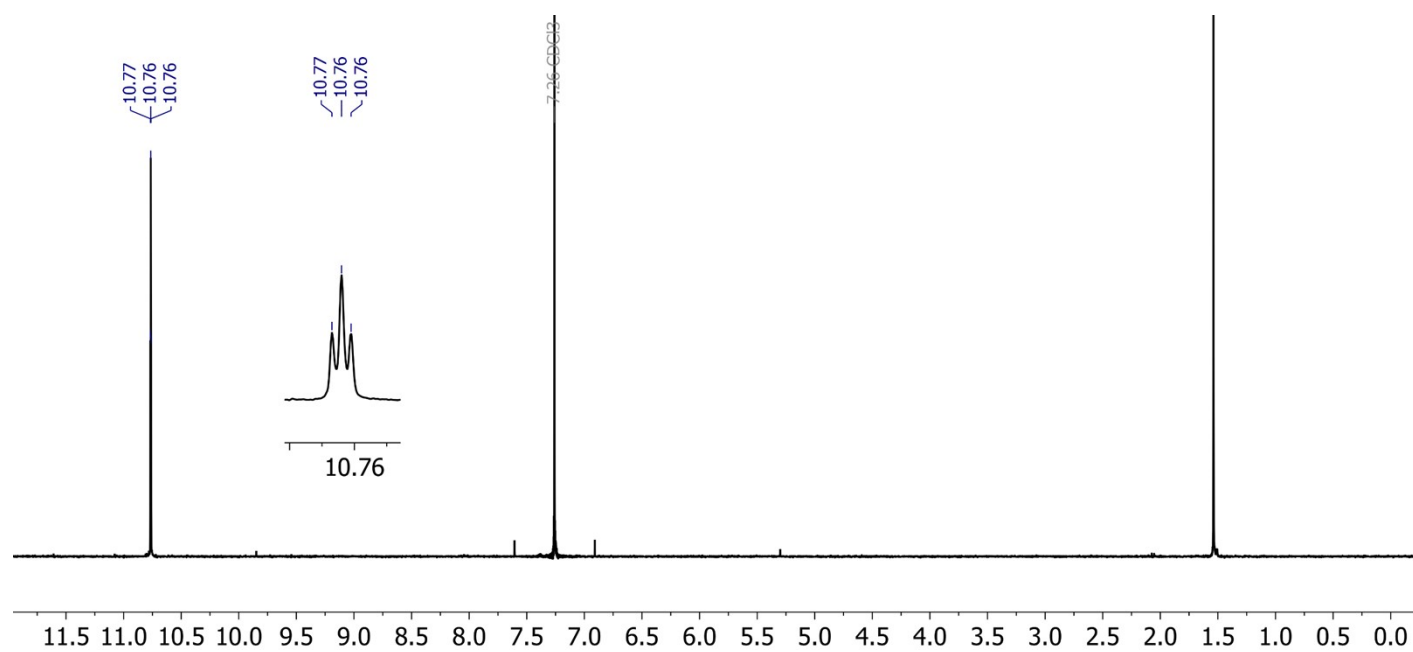
Figure S15. ^1H NMR (300 MHz, CDCl$_3$) spectrum of **8**.
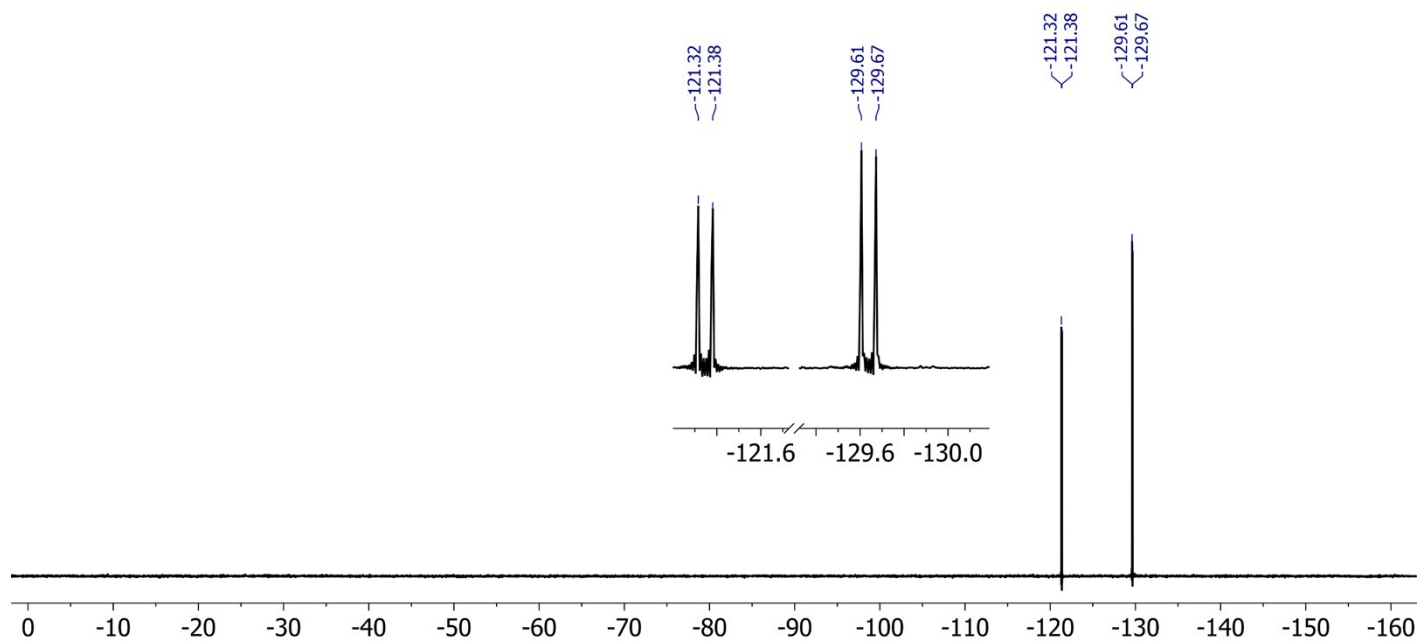
Figure S16. ^{19}F NMR (282 MHz, CDCl$_3$) spectrum of **8**.
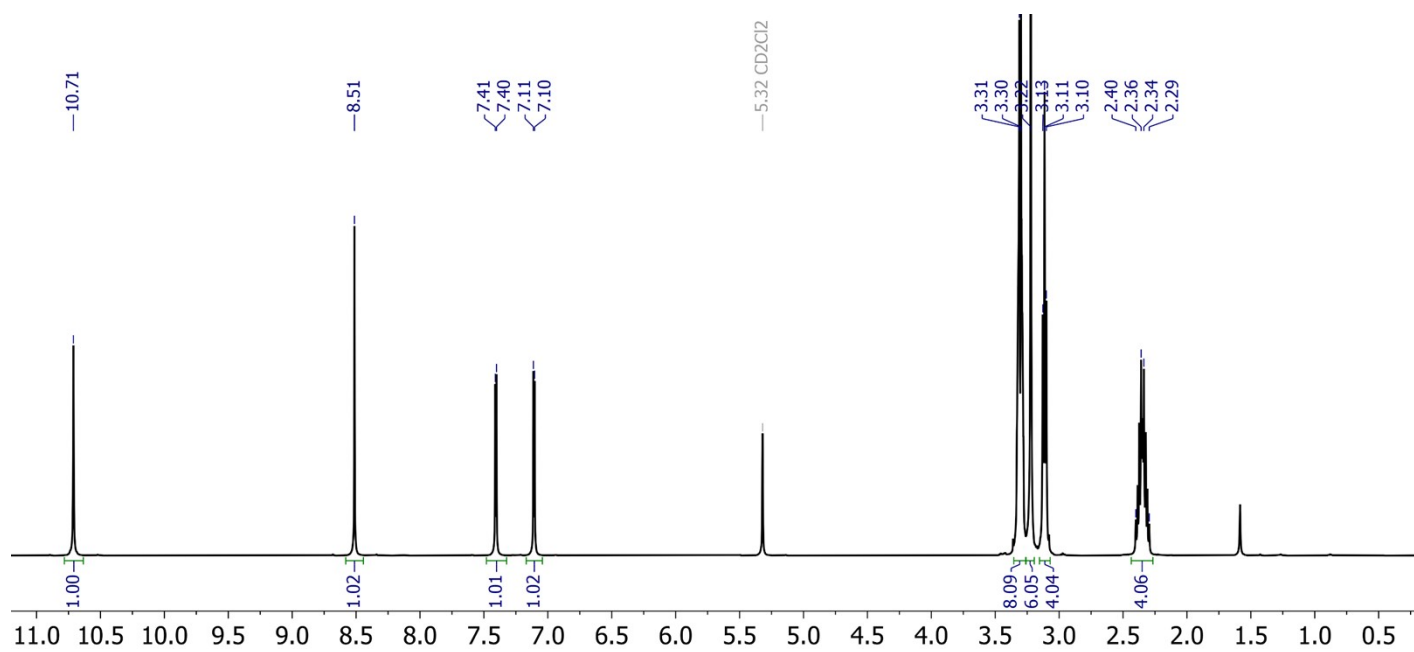
Figure S17. ^{1}H NMR (500 MHz, CD$_2$Cl$_2$) spectrum of **CPDT-DFBT-Ald**.
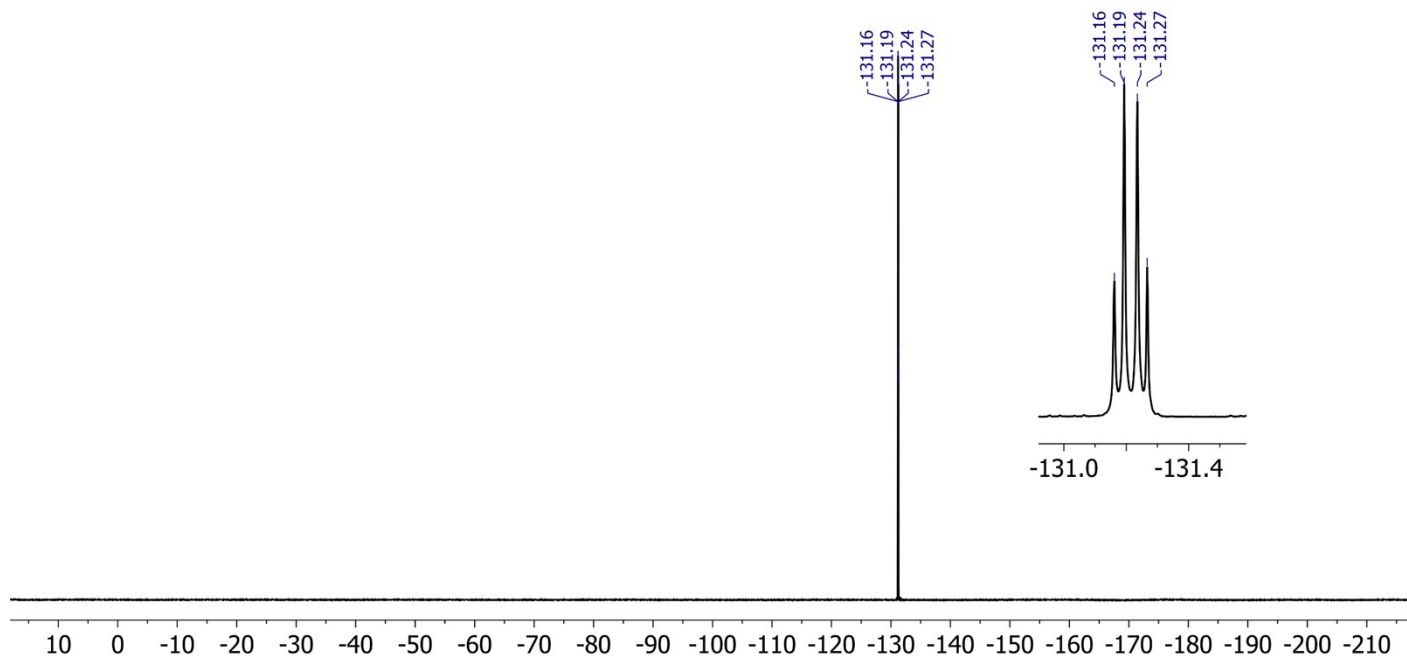
Figure S18. ^{19}F NMR (470 MHz, CD$_2$Cl$_2$) spectrum of **CPDT-DFBT-Ald**.

Figure S19. ^{13}C{^{1}H} NMR (126 MHz, CD$_2$Cl$_2$) spectrum of **CPDT-DFBT-Ald**.

Figure S20. Expansion of the aromatic region of the $^{13}C\{^1H\}$ NMR (126 MHz, CD_2Cl_2) spectrum of **CPDT-DFBT-Ald**. The signal at 125.26 ppm is due to dissolved carbon dioxide.
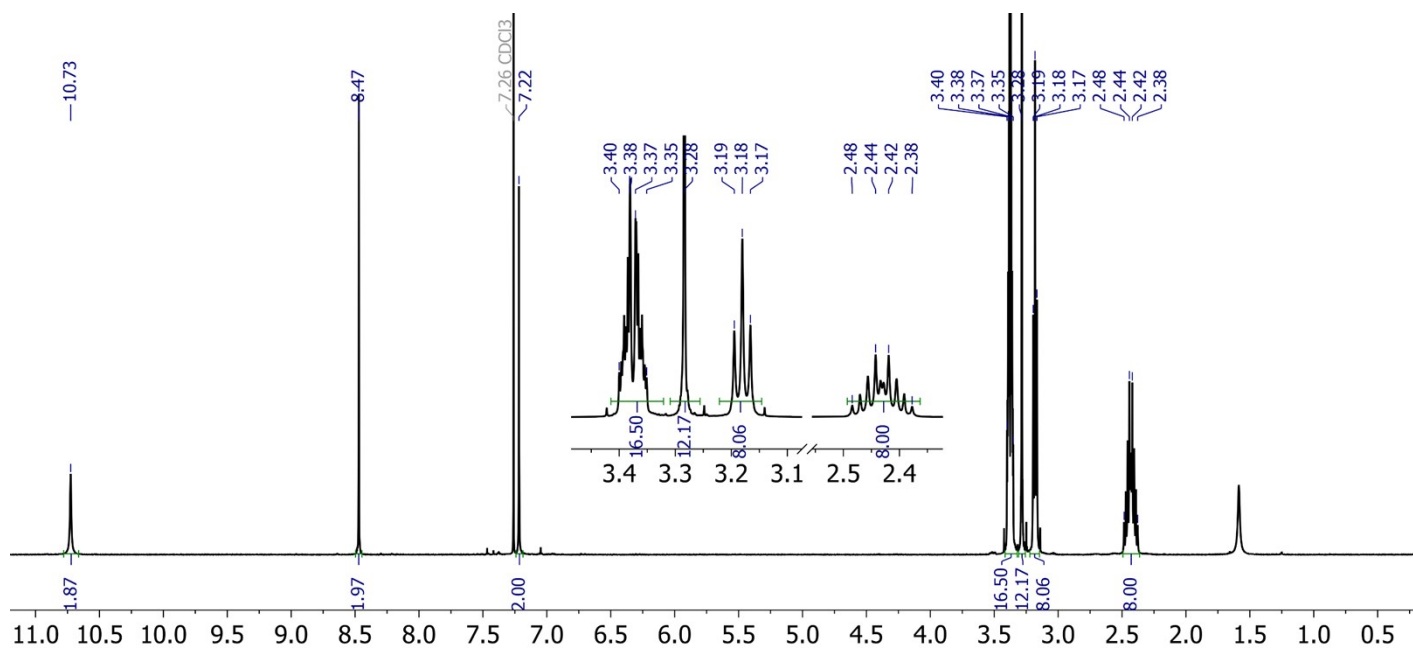
Figure S21. ^1H NMR (500 MHz, $CDCl_3$) spectrum of **D(CPDT-DFBT-Ald)**.
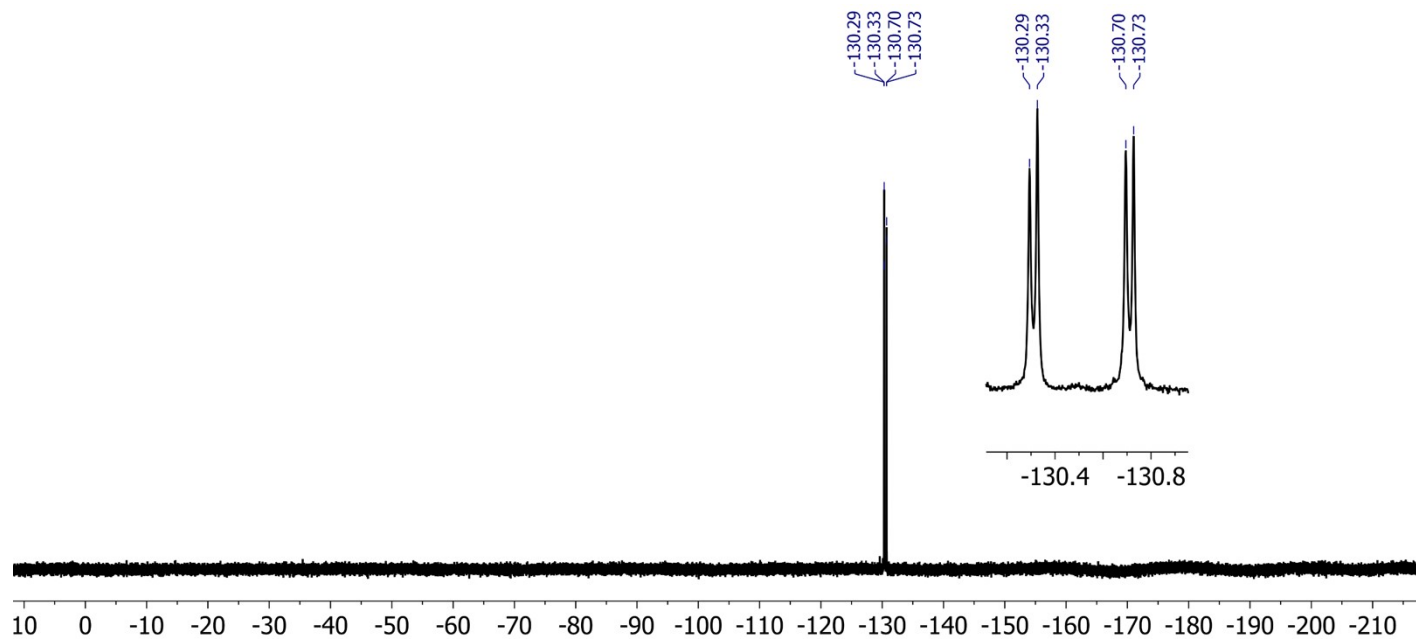
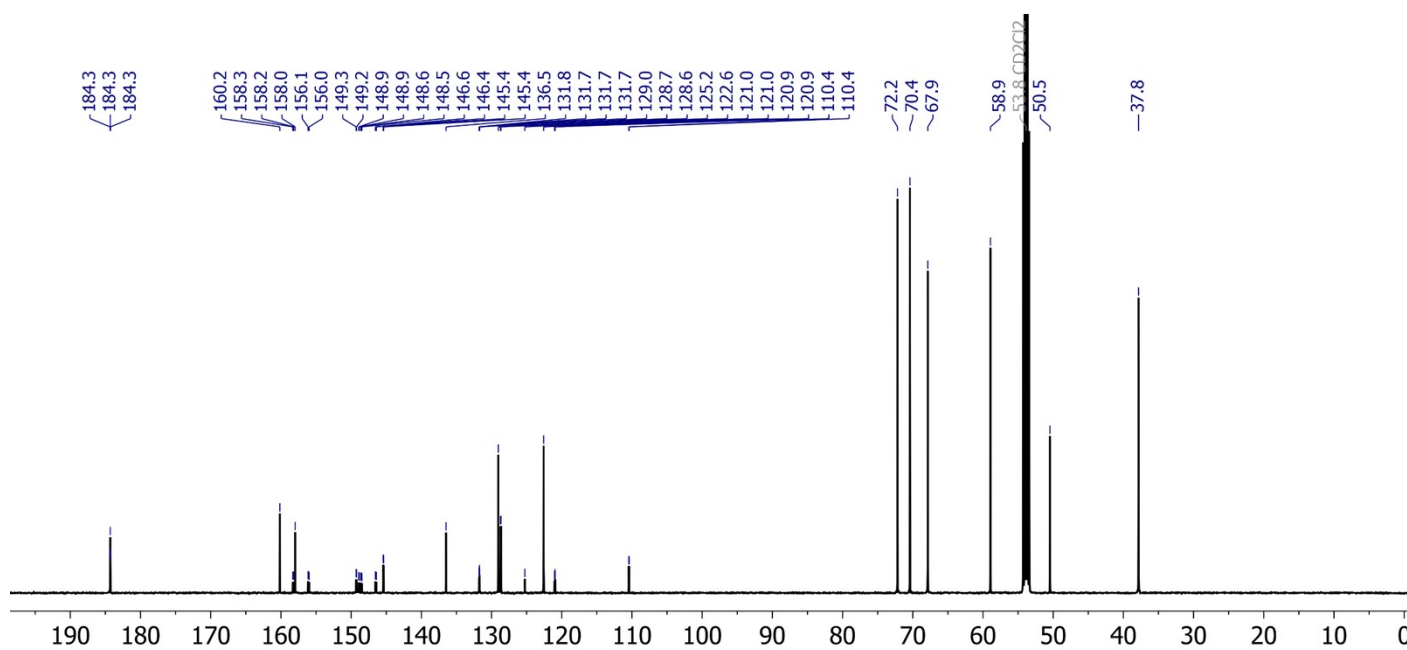**Figure S22.** ^{19}F NMR (470 MHz, CDCl$_3$) spectrum of **D(CPDT-DFBT-Ald)**.

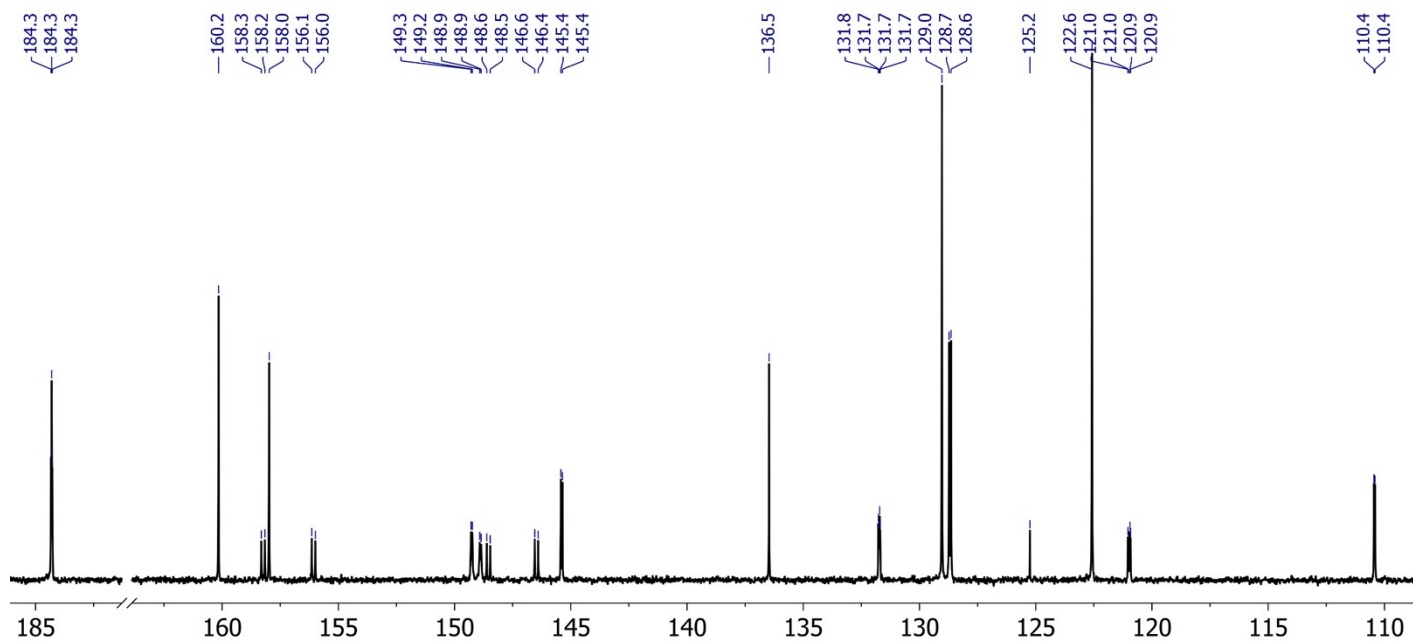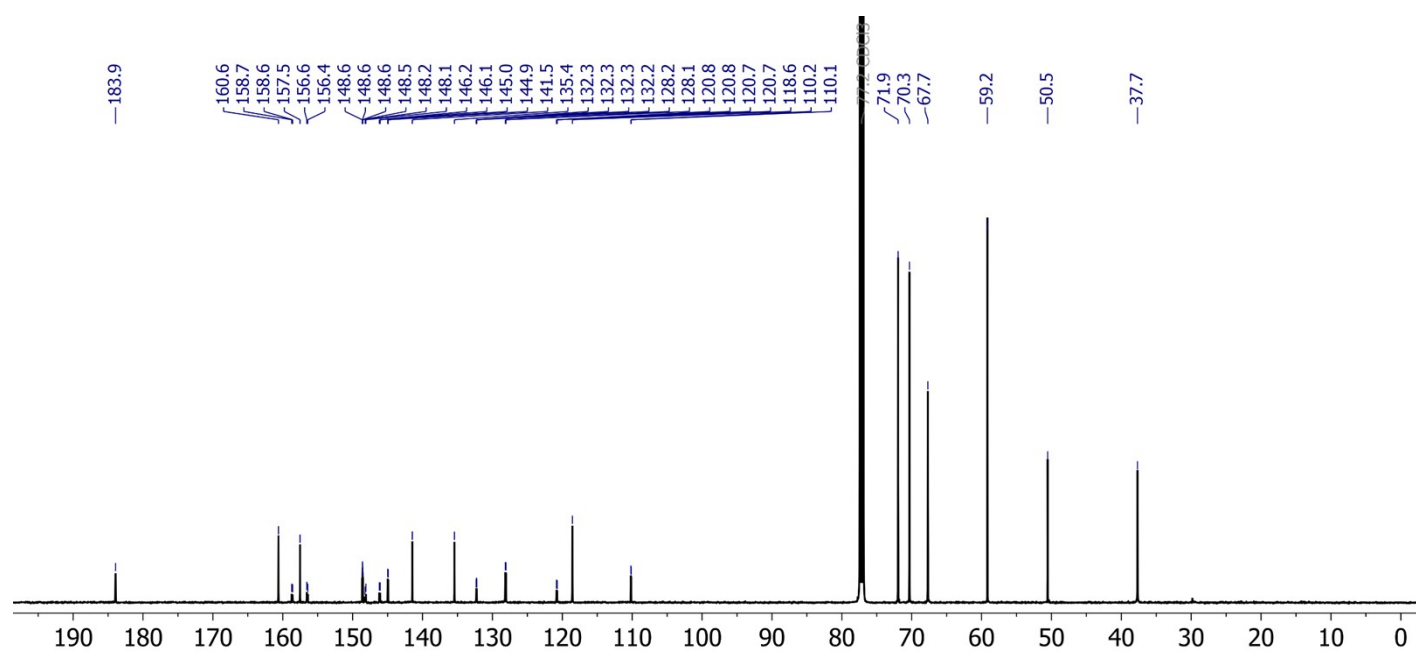**Figure S23.** $^{13}C\{^1H\}$ NMR (126 MHz, CDCl$_3$) spectrum of **D(CPDT-DFBT-Ald)**.
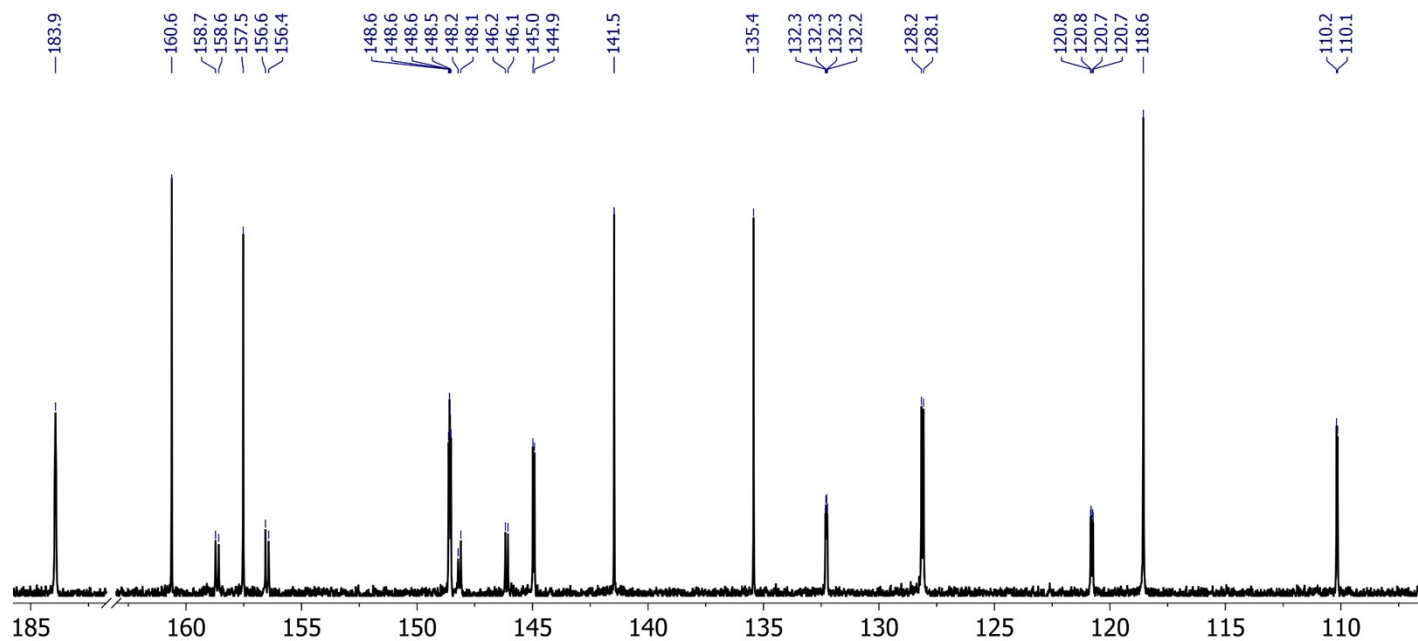
Figure S24. Expansion of the aromatic region of the $^{13}C\{^1H\}$ NMR (126 MHz, CDCl$_3$) spectrum of **D(CPDT-DFBT-Ald)**.

Differential scanning calorimetry
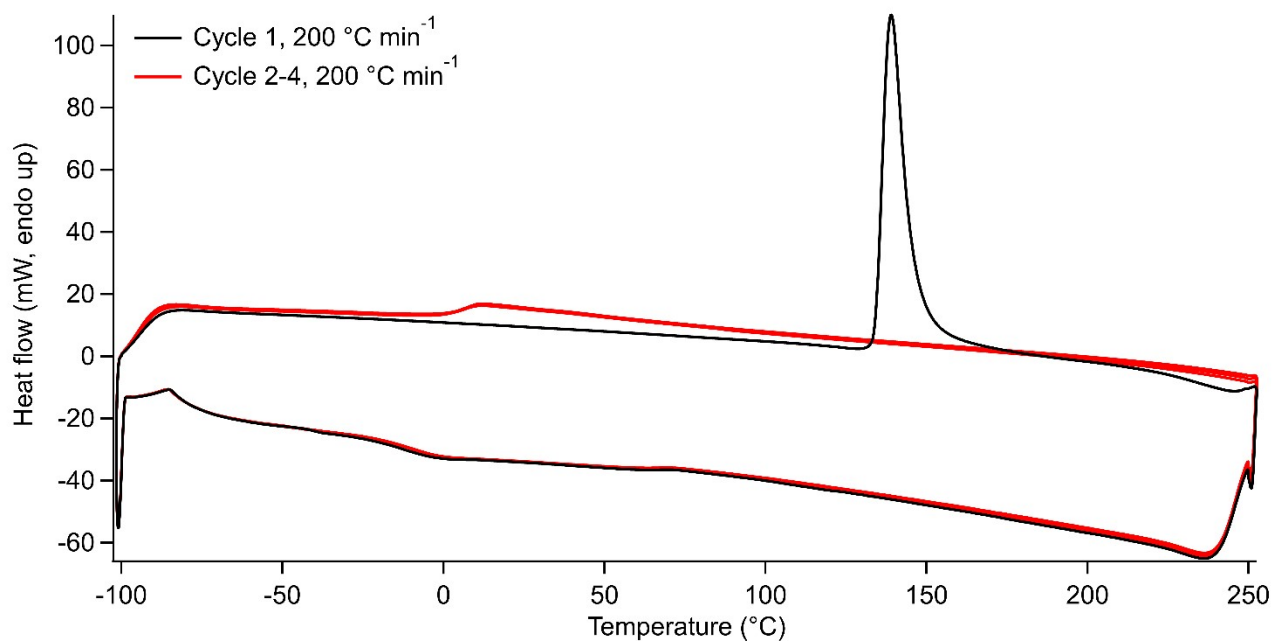
Figure S25. The DSC thermogram of **CPDT-BT-Ald**, measured at a scan rate 200 °C min^{-1}. The first heating/cooling cycle is plotted in black, subsequent cycles are plotted in red.
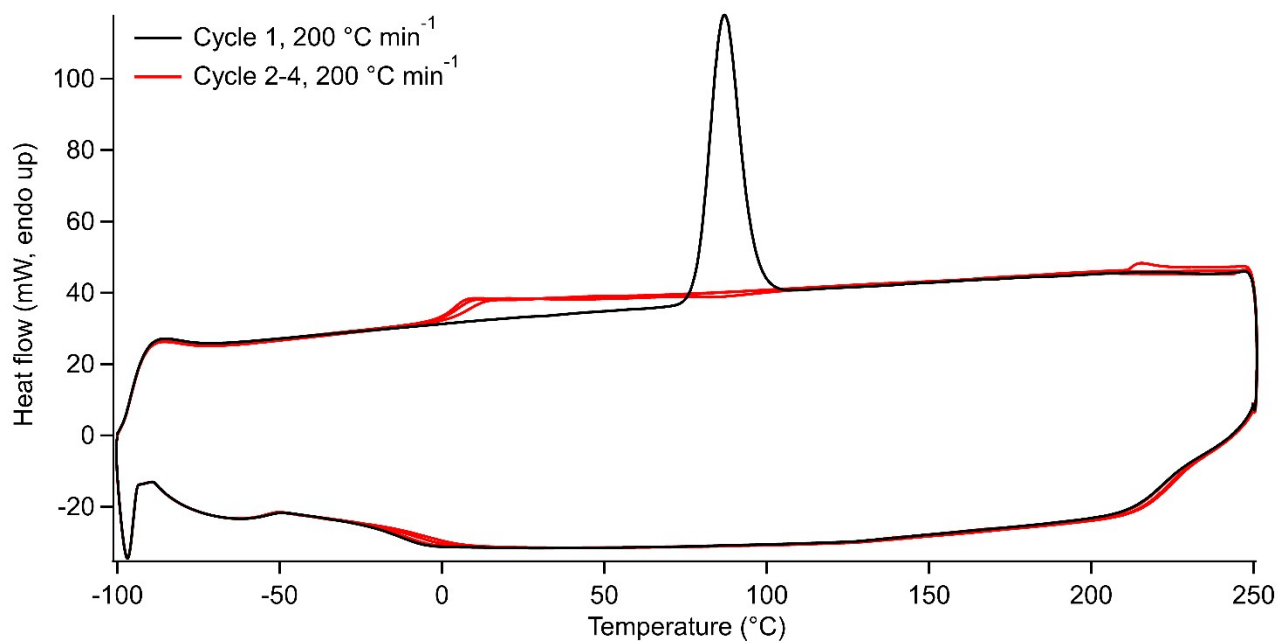
Figure S26. The DSC thermogram of **CPDT-DFBT-Ald**, measured at a scan rate 200 °C min^{-1}. The first heating/cooling cycle is plotted in black, subsequent cycles are plotted in red.
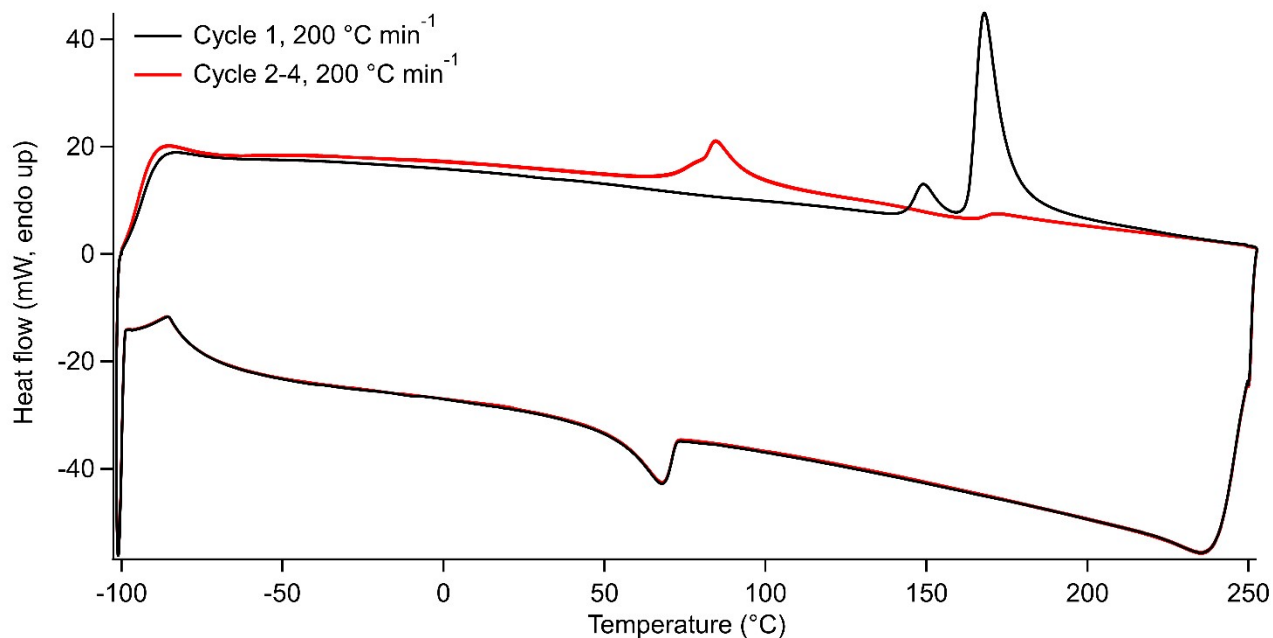
Figure S27. The DSC thermogram of **D(CPDT-BT-Ald)**, measured at a scan rate 200 °C min^{-1}. The first heating/cooling cycle is plotted in black, subsequent cycles are plotted in red.

Figure S28. The DSC thermogram of **D(CPDT-DFBT-Ald)**, measured at a scan rate 200 °C min^{-1}. The first heating/cooling cycle is plotted in black, subsequent cycles are plotted in red.

Figure S29. Grazing-incidence X-ray diffraction (GIXRD) graphs of aged films of a) **CPDT-BT-Ald**, b) **CPDT-DFBT-Ald**, c) **D(CPDT-BT-Ald)** and d) **D(CPDT-DFBT-Ald)**. The data was collected out-of-plane at an incidence angle of 0.3°.

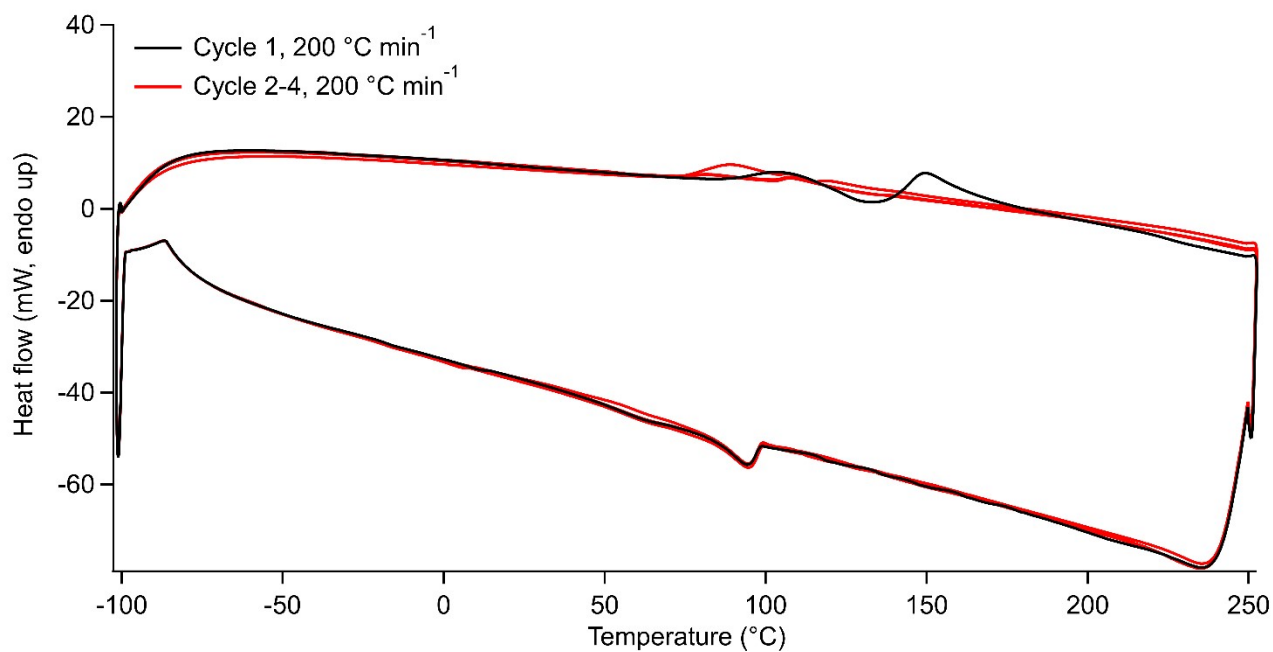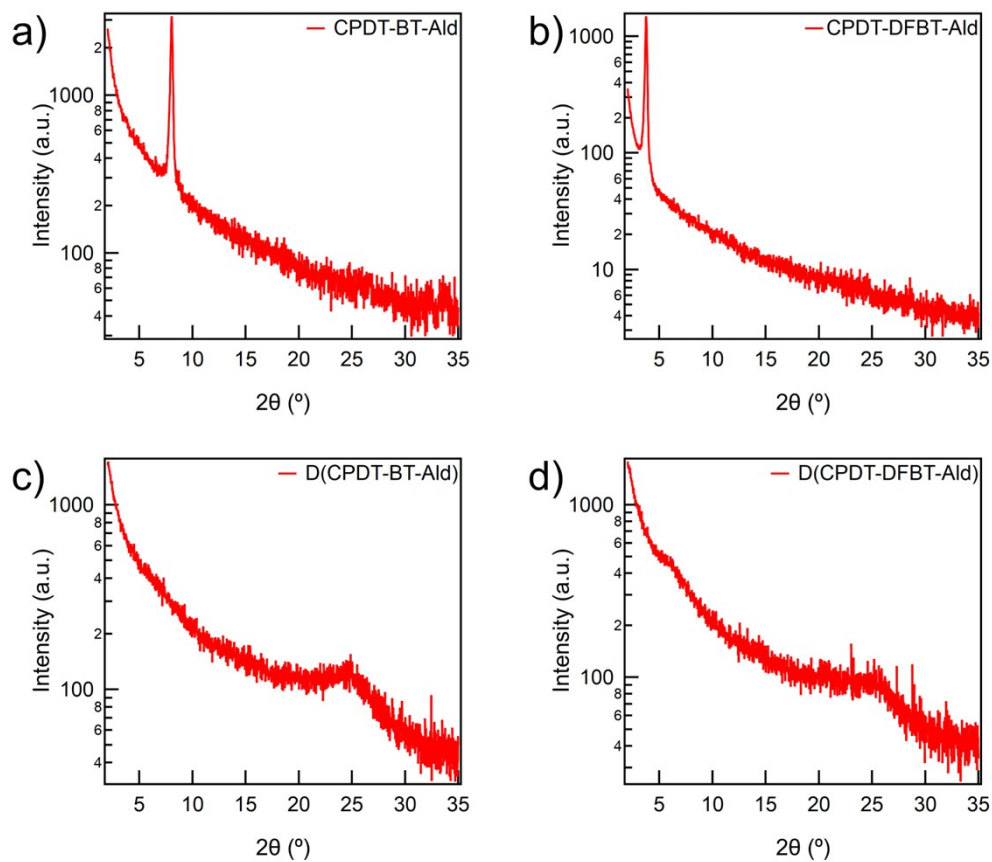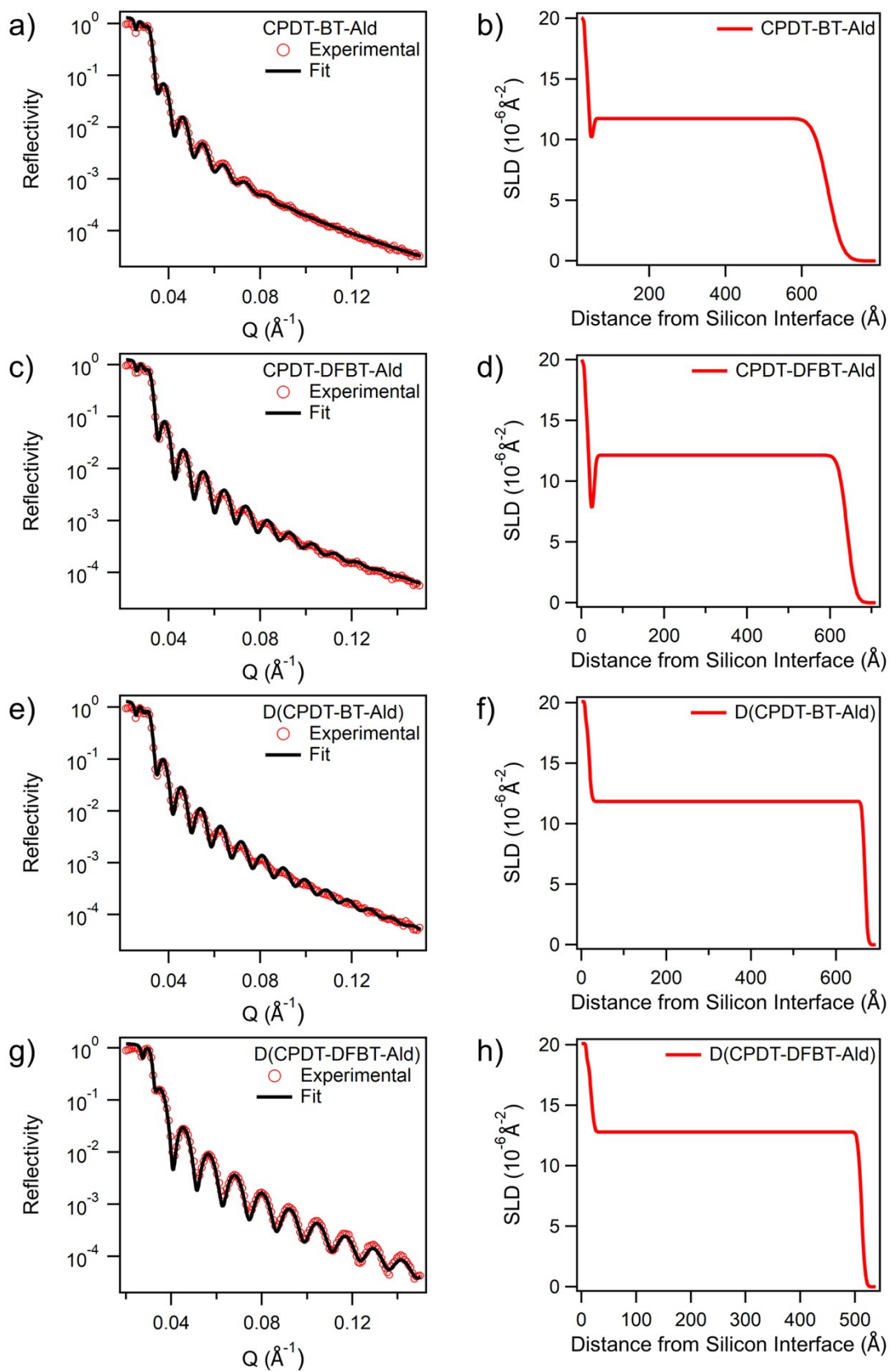**Figure S30.** X-ray reflectometry profiles and fits (left) and corresponding scattering length density profiles (right) of **CPDT-BT-Ald** (a, b), **CPDT-DFBT-Ald** (c, d), **D(CPDT-BT-Ald)** (e, f) and **D(CPDT-DFBT-Ald)** (g, h). Measurements were performed on amorphous, freshly cast films.

Table S1. Summary of the X-ray reflectometry results, obtained from measurements on freshly cast films. The thickness and scattering length density are determined by a model fit to the experimental data. The density is calculated from the fitted scattering length density.

Compound	Thickness (nm)	Scattering length density (10^{-6} Å^{-2})	Density (g cm^{-3})
CPDT-BT-Ald	61.8	11.8	1.31
CPDT-DFBT-Ald	61.2	12.1	1.36
D(CPDT-BT-Ald)	65.0	11.85	1.32
D(CPDT-DFBT-Ald)	49.4	12.79	1.44

Electrochemistry
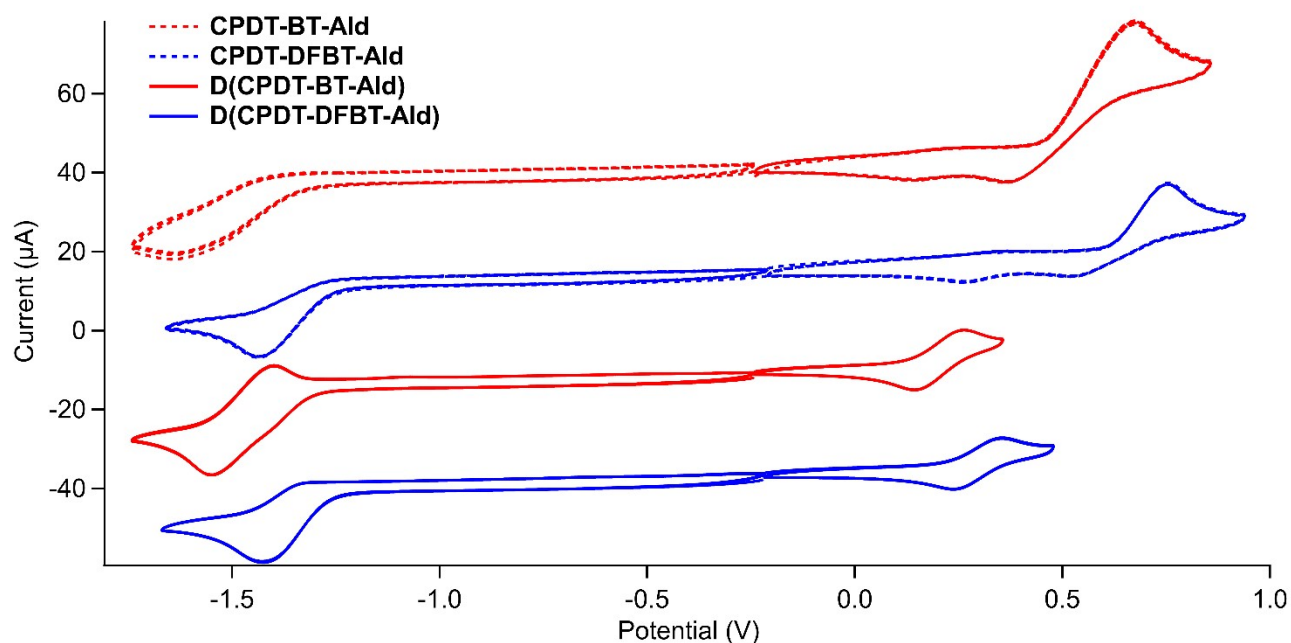
Figure S31. Stacked cyclic voltammograms (dichloromethane, 0.1 M tetrabutylammonium perchlorate) of the compounds, offset in the y-axis for clarity. Oxidation and reduction cycles were measured separately. Four full cycles of each are shown. The data was collected at a scan speed of 50 mV s^{-1} and referenced against the

ferrocene/ferrocenium couple. The $E_{\frac{1}{2}}$ of the reductions were confirmed using differential pulse voltammetry when a clear anodic peak for the reduction was not observed.
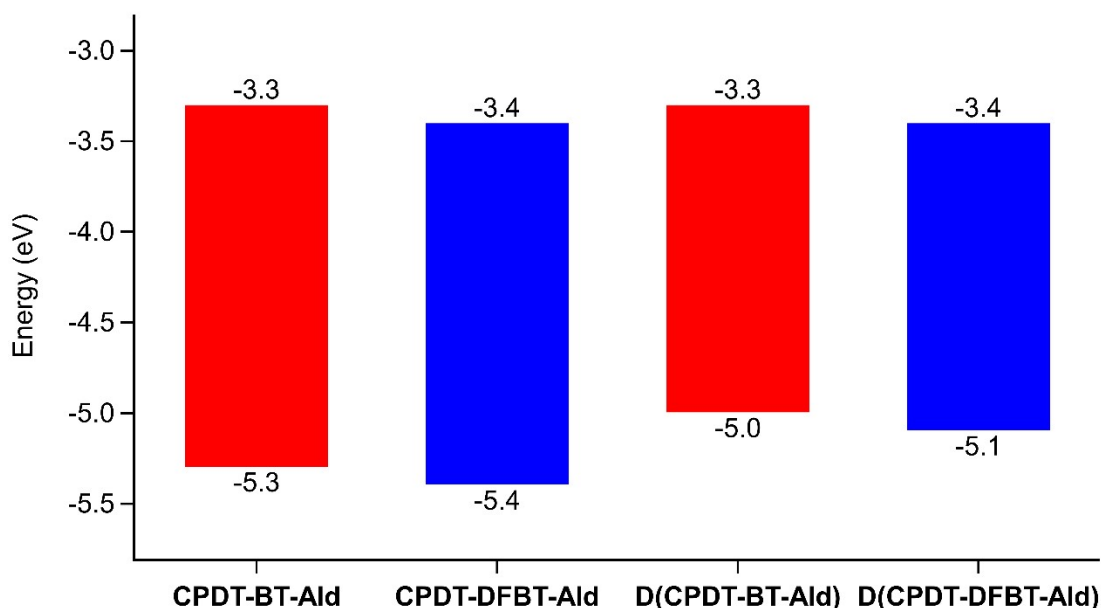
Figure S32. Estimated ionisation potentials and electron affinities calculated from the cyclic voltammetry $E_{\frac{1}{2}}$s (dichloromethane, 0.1 M tetrabutylammonium perchlorate, referenced against the ferrocene/ferrocenium couple), rounded to the nearest 0.1 eV. Ferrocene was taken as having an ionisation potential of 4.8 eV.
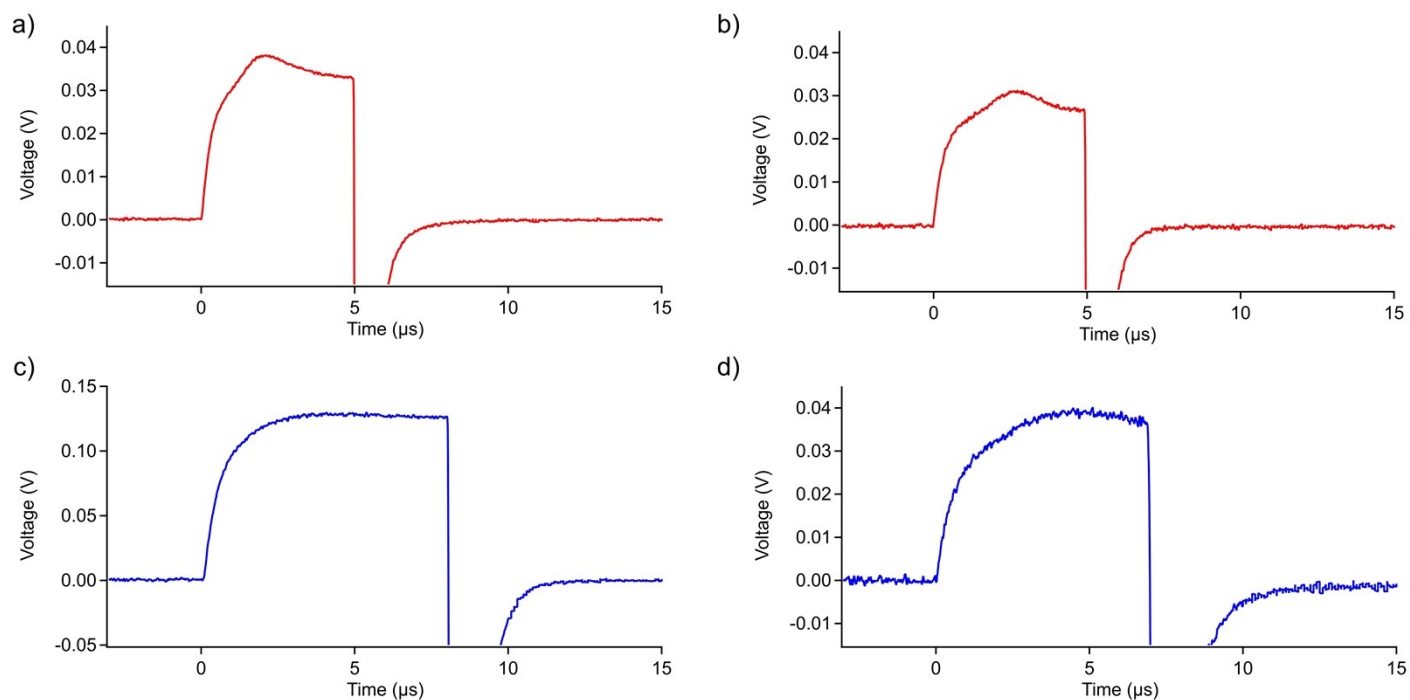
Figure S33. Electron and hole carrier transients for **D(CPDT-BT-Ald)** (a and b, respectively) and **D(CPDT-DFBT-Ald)** (c and d, respectively) measured using MIS-CELIV.

Device fabrication and testing

15 mm × 15 mm 15 Ohm square^{-1} ITO-coated glass substrates (Xinyan, Hong Kong) were cleaned in an Alconox solution at 70 °C before being sonicated in sequence with Alconox, de-ionised water, acetone and *iso*-propanol for 10 minutes each, followed by drying with pressurised nitrogen. The substrates were then treated in a UV-Ozone system for 20 min. The hole transport layer was prepared by filtering poly(3,4-ethylenedioxythiophene):polystyrene sulfonate (PEDOT:PSS AI 4083) through a 0.45 µm filter before spin-coating the solution in air at 5000 rpm and annealing at 150 °C for 20 min in air to produce a 30 nm film. Solutions of **D(CPDT-BT-Ald)** and **D(CPDT-DFBT-Ald)** at a concentration of 10 mg mL^{-1} were prepared in chloroform. All active layers were spin-coated in a nitrogen-filled MBraun glovebox (oxygen and water concentrations of < 1 ppm) onto the ITO/PEDOT:PSS substrates at 2000 rpm to produce films with thicknesses of 40–50 nm. The film thicknesses were measured with a Bruker DektakXT profilometer. Finally, 10 nm of bathocuproine (BCP), 25 nm of calcium (Ca), and 100 nm of silver (Ag) were sequentially thermally deposited through a shadow mask under a 10^{-6} mbar vacuum. The final effective area for each device was 0.08 cm^2 with four complete devices prepared on each substrate.

The devices were tested in a nitrogen filled MBraun glove box with oxygen and water concentrations of < 1 ppm. Current-voltage (*J-V*) characteristics were acquired using a Keithley 2400 Source Measurement Unit with a 4-wire configuration to eliminate the effect of the cable resistances and the internal impedance of the SMU. A Newport Sol3A AM 1.5G solar simulator was used to simulate Air Mass 1.5 Global (AM 1.5 G) illumination. The illumination intensity of 1 sun used for the organic solar cell measurements was set using a Newport-calibrated meter in conjunction with an unfiltered silicon reference cell. The *J-V* curves were measured on at least four devices for statistics. A 0.08 cm^2 shadow mask was applied to each device during testing.

The external quantum efficiency (EQE) spectra were recorded with a PV Measurement QEX7 setup, which was calibrated using an NREL-certified photodiode and operated without white-light bias and chopped and locked in the small perturbation limit. EQE measurements were performed from 400 nm to 1000 nm.
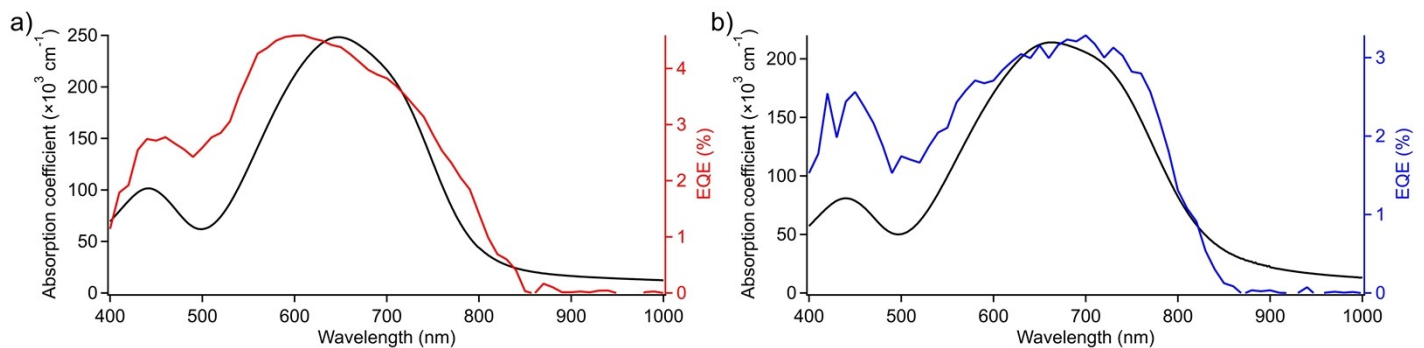

Figure S34. Thin-film absorption spectra and external quantum efficiency (EQE) of the homojunction devices with a structure of ITO/PEDOT:PSS/homojunction/BCP/Ca/Ag composed of **D(CPDT-BT-Ald)** (a) and

D(CPDT-DFBT-Ald) (b).
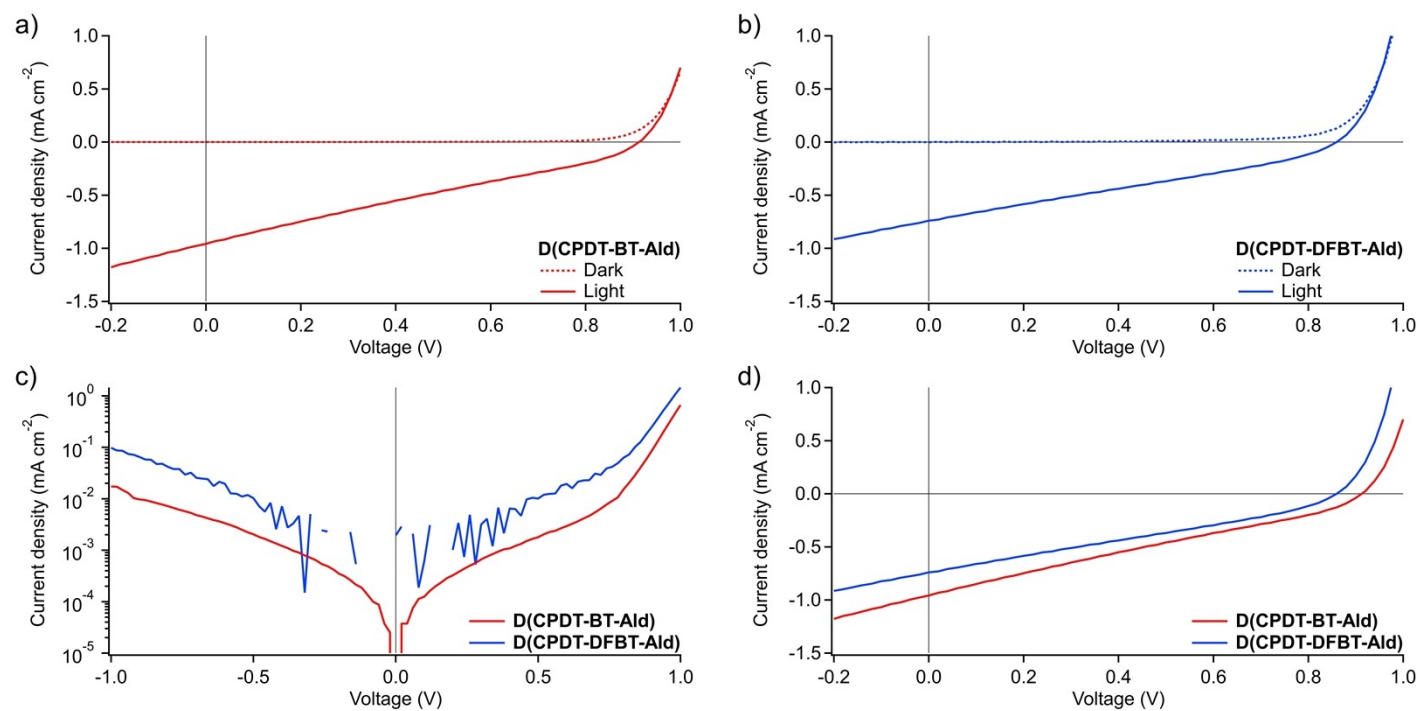

Figure S35. Current density versus voltage (*J-V*) characteristics in the dark and under illumination of 100 mW cm^{-2} for devices composed of **D(CPDT-BT-Ald)** (a) and **D(CPDT-DFBT-Ald)** (b), along with the comparison of the two dimers in semi-log *J-V* in the dark (c) and under illumination (d).